Manuscript Details

Manuscript number	SUBMIT2IJMS_2019_2291_R1
Title	A novel test method for continuous nonlinear biaxial tensile deformation of sheet metals by bulging with stepped-dies
Article type	Research Paper

Abstract

In this paper, a novel test method named bulging with stepped-dies is proposed to overcome the difficulty of traditional test methods in realizing continuous nonlinear loading paths from initial yield up to fracture on a sheet metal. To achieve this aim, the section shape of a stepped-die cavity is varied with increasing depth. During bulging with a stepped-die, the stress state at the pole of bulging area of the sheet changes continuously with the increase in bulging height, which results in a specific nonlinear loading path. A theoretical model is established to calculate the stress components at the pole based on the assumption that the bulged surface near the pole was approximated by a rotational ellipsoid. Bulging experiments with three different stepped-dies are performed by using ST16 steel sheet. Stress and strain paths up to fracture and equivalent stress-strain curves at the pole are analyzed and compared with the results of bulging with elliptical dies. It is shown that continuous nonlinear loading paths can be effectively realized through bulging with stepped-dies and the stress ratio at the pole changes from 0.5 up to 2.0 at most in one bulging experiment. The feasibility of the novel test method is validated successfully. And the experimental data obtained are useful to determine constitutive and forming limit models suitable for complex loading conditions.

Keywords	nonlinear loading; biaxial tensile; stepped-die; bulge test; forming limit
Taxonomy	Mechanical Property, Forming Process, Materials Testing
Manuscript category	MATERIAL PROCESSING

Corresponding Author	Zhubin He
Corresponding Author's Institution	Harbin Institute of Technology
Order of Authors	Zhubin He, Haihui Zhu, Yanli Lin, Denis Politis, Liliang Wang, Yuan Shijian

Submission Files Included in this PDF

File Name [File Type]

Cover letter-r1.docx [Cover Letter]

Response to Reviewers.docx [Response to Reviewers]

Highlights.docx [Highlights]

Graphical abstract-r1.tif [Graphical Abstract]

IJMS-Manuscript-Revised.docx [Manuscript File]

declaration of competing interests.docx [Conflict of Interest]

To view all the submission files, including those not included in the PDF, click on the manuscript title on your EVISE Homepage, then click 'Download zip file'.

Dear Prof. Davey:

On behalf of my co-authors, we thank you very much for giving us an opportunity to revise our manuscript, and we appreciate editors and reviewers very much for their positive and constructive comments and suggestions on our manuscript entitled “A novel test method for continuous nonlinear biaxial tensile deformation of sheet metals by bulging with stepped-dies” for possible publication in your famous journal “International Journal of Mechanical Sciences”. (Ref: **SUBMIT2IJMS_2019_2291**).

We have studied reviewers’ comments carefully and have made revision which marked in red in the paper. The responses to the reviewers’ comments are given point by point in the document “Response to Reviewers”. Attached please find the revised version, which we would like to submit for your kind consideration.

Moreover, we hope to get your approval for the **changes to authorship** of our revised manuscript. With the agreement of all authors, we want to change the corresponding author from Haihui Zhu to his associate supervisor Prof. Zhubin He, and to add Dr. Denis J. Politis as the fourth author. Reasons are as follows:

This work was mainly supported by the National Natural Science Foundation of China (No. 51575131). Prof. Zhubin He is the leader of this project. The project has been transferred from Harbin Institute of Technology to Dalian University of Technology, where Prof. Zhubin He works now. As a Ph.D. student at Harbin Institute of Technology, it is no longer convenient for Haihui Zhu to be the corresponding author. More importantly, Prof. Zhubin He will continue to study this topic in the future as the leader. Therefore, changing the corresponding author to Prof. Zhubin He is not only convenient to contact but also responsible for the research.

Dr. Denis J. Politis contributed much in the revised manuscript. He modified the theoretical model in section 2.2 to considering the effect of the bending strains. And he re-wrote the descriptions of the stepped-dies used in the manuscript in a way that is easier to understand. Due to Dr. Denis J. Politis’ contribution, he should be added to the author list.

Once again, we deeply appreciate you and reviewers for the great efforts that help us improve our manuscript.

Looking forward to hearing from you.

With kind regards,

Yours sincerely,

Dr. Prof. Zhubin He

a) School of Materials Science & Engineering, Harbin Institute of Technology, Harbin

150001, P.R. China
b) School of Mechanical Engineering, Dalian University of Technology, Dalian 116024, P.R. China
Tel: +86-15244629678
Email: hithe@hit.edu.cn

Dear Editors and Reviewers,

Thank you for your letter and for the reviewers' comments concerning our manuscript entitled "A novel test method for continuous nonlinear biaxial tensile deformation of sheet metals by bulging with stepped-dies" for possible publication in the famous journal "International Journal of Mechanical Sciences". (**Ref: SUBMIT2IJMS_2019_2291**). Those comments are all valuable and have been incorporated into the revised paper. The revised portions have been marked in red. The responses to the reviewers' comments are as follows:

Responses to Reviewer 1:

1. What are differences between your new approach and the traditional bulging test method for example see the following paper: Utilization of bulge and uniaxial tensile tests for determination of flow stress curves of selected anisotropic alloys.

Response:

Thank the reviewer for the valuable question. We have studied the paper "Utilization of bulge and uniaxial tensile tests for determination of flow stress curves of selected anisotropic alloys" in depth, and this paper has been referred to in the Introduction paragraph 3 with reference number [13]. The differences between the new approach and the traditional bulging test method have also been added in section 4.6 paragraph 1, as follows:

"The new method, bulging with stepped-dies, was developed based on the traditional bulging test method. The key development in this work is that the section shape of a stepped-die cavity varies as the depth increases, which is different from the monotonous elliptical or circular die section in the traditional method. As a result, continuous nonlinear loading paths can be realized."

2. Some recent references which discussed nonlinear loadings or bulging test could be mentioned in the article such as: "Experimental and theoretical investigation of strain path change effect on forming limit diagram of AA5083" and "An Experimental, Analytical, and Numerical Investigation of Hydraulic Bulge Test in Two-Layer Al–Cu Sheets"

Response:

Thank the reviewer for recommending two papers to us. The methods and conclusions in these two articles are interesting and have been included in the manuscript. The first paper has been added in the Introduction paragraph 2 and 5 as reference [5], and the second paper has been added in the Introduction paragraph 3 as reference [12]. Descriptions of the finding of

these papers have also been added.

3. Please add the detailed mechanical properties of ST16 to the paper.

Response:

Thank the reviewer for the suggestion, and we have added the detailed mechanical properties of ST16 have been added in Fig. 3 and Table 2. The true stress-strain curves in 0°, 45° and 90° angles measured from RD are shown in Fig. 3. Moreover, the yield stresses (σ_s), ultimate tensile strength (σ_{uts}), Lankford coefficients (r), hardening coefficient (K) and strain-hardening exponent (n) at 0°, 45° and 90° are listed in Table 2.

4. Please add a figure which shows the specimen and configuration of specimen for the uniaxial tensile test.

Response:

Based on the reviewer's suggestion, the figure for the configuration of the specimen for the uniaxial tensile tests has been added in Fig. 3. The specimen was designed according to the testing standard GB/T 228.1-2010 with descriptions added to section 3.1 paragraph 2.

5. What is your software for used DIC technique?

Response:

The software used in this paper was XTDIC 3D full-field strain measurement and analysis system, developed by Xi'an Jiaotong University. A description of the DIC technique has been added in section 3.2, paragraph 1.

6. Why did the stress-strain curves which obtained from bulging test show more elongation than that of obtained from uniaxial tensile test (e.g., Fig. 13)?

Response:

This is a very interesting question. A similar phenomenon was also found in Aluminum alloy and Titanium alloy, as shown in Figure 19 in the paper "Utilization of bulge and uniaxial tensile tests for determination of flow stress curves of selected anisotropic alloys" published by Janbakhsh et al. And the reference to this paper has been added to the introduction paragraph 3 of the revised manuscript with number [13].

There are two major reasons for the phenomenon:

(1) From Fig. 14 (the original Fig. 13) it can be seen that the stress-strain curves obtained from the bulging test are higher than that obtained from the uniaxial tensile test, which means the ST16 sheet exhibits higher strain-hardening exponent (n) during bulging test. Generally,

higher strain-hardening exponent delays the onset of instability, and leads to a greater limit strain. This was also mentioned in the section Results and Discussion of reference [13], where the mechanical properties of different sheet materials were compared.

(2) The end of the stress-strain curve obtained from uniaxial tensile test shown in Fig.14 is diffuse necking, corresponding to the maximum tensile force. After necking, a large degree of deformation continues until fracture occurs. The curve after necking is not given as the deformation after necking is not uniform and the true stress cannot be calculated accurately. On the other hand, the end of the stress-strain curve obtained from the bulging test is fracture of the specimen. Meanwhile, the deformation from necking to fracture is not so apparent because the necking occurs late and evolves into fracture rapidly. Therefore, if the curve of uniaxial tensile after necking is considered, the difference of elongation between uniaxial tensile test and bulging test will be greatly reduced.

However, considering that the difference of elongation does not affect the focus of the current paper, the explanations above are not given in the revised manuscript.

Responses to Reviewer 2:

1. How the stepped bulge die is designed? And how did you calculate the dimensions of stepped bulge die sections? I mean, before doing the experimental tests, on what principles were you sure that the desired stress condition was obtained in the for your test setup. Given that there is no specific standard for your test setup.

Response:

As the reviewer has identified the design method for a stepped-die has not been standardized. The main purpose of the current work was to verify the feasibility of the novel test method and the effect of basic designs on the change of stress and strain paths at the pole point during bulging with stepped-dies. Having developed the test method and theoretical model in the current paper, the authors intend in a subsequent study to develop design strategies for the stepped-die to induce the required user defined stress and strain paths.

Moreover, the three stepped-dies used in the current work were designed for the typical nonlinear loading path, i.e. an equal biaxial tension followed by unequal biaxial tension. The variation parameters were the deformation level in step I and the section shape in step II. In the revised manuscript, the description of the stepped-dies has been revised incorporating the use of notation such as $S^{0.1}_{1-0.4}$ added in section 3.3 paragraph 2. And further details of the three stepped-dies used in the current work have been added in Table 3.

2. From a plasticity standpoint, please explain clearly why the material failure into larger equivalent stress in the nonlinear loading path of bulging with stepped-dies, (could it be related to the multi-stage forming?)

Response:

Thank the reviewer for the valuable comment. According to the paper "Extension of homogeneous anisotropic hardening model to cross-loading with latent effects" performed by Barlat et al. [46], the latent hardening effect is clearly identified in the EDDQ steel. The effect can lead to flow stress overshoot during two-step tension testing. As both ST16 and EDDQ steel belong to interstitial-free steel, ST16 should also exhibit the property of latent hardening. Due to the latent hardening effect, the equivalent stress of ST16 during step II of bulging with stepped-dies overshoots that of bulging with the circular die.

The explanation above has been added into the last paragraph of section 4.5. And the paper has been added as reference [46].

3. I think the pressure path in the new stepped-dies differs from the pressure path in the elliptical bulge dies, and one of the reasons for the nonlinearity of the stress state is the non-linearity of the stepped-dies pressure path. Please include two pressure path curves in the article and compare them.

Response:

Based on the reviewer's suggestion, a more detailed model for stress components considering the pole thickness was developed and presented in section 2.2.1 of the revised manuscript. According to the stress analysis at the pole point and Eqs. (4) and (5) mentioned in section 2.2.1, the stress ratio is dependent on the two principle curvature radii ρ_{RD} and ρ_{TD}, and the pole thickness t, but is irrelevant to the bulging pressure p. On the other hand, the pressure causing the sheet metal to yield is a dependent variable determined by the yield strength and the two principle curvature radii of the bulged sheet. Therefore, the pressure path will not lead to nonlinearity of the stress state.

The pressure paths obtained from bulging with a circular die, an elliptical die and a stepped-die are shown in the figure below. However, considering the pressure paths have no effect on the nonlinearity of the stress state, the pressure paths are not added into the revised manuscript.

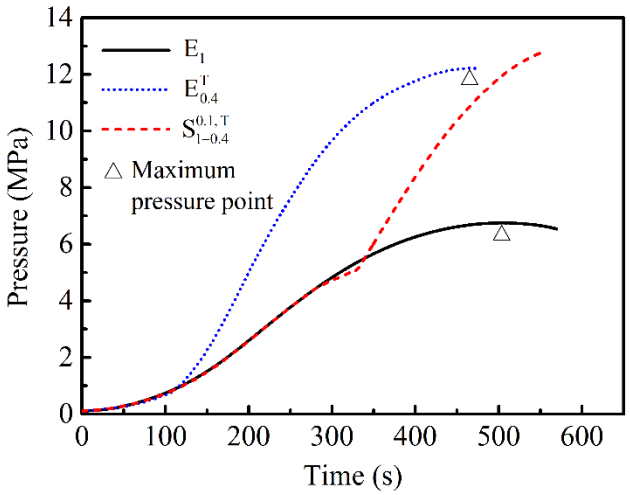

Fig. 1 Pressure paths during bulging with a circular die, an elliptical die and a stepped die.

4. How do you explain the difference in the amount of stress and strain at the point of failure in the presented bulge die and elliptical die? In the article comes out" the difference illustrates the path-dependence of the forming limit strains in sheet metal forming" but based on research by Korkolis et al[1] " It is confirmed that failure strains are path-dependent, but also is demonstrated that failure stresses become path-dependent if the pre-strain is significant." Have you considered this point in your study? Please add a comment in the article.

Response:

Thank the reviewer for the valuable comment. The authors have read the research "Path-dependent failure of inflated aluminum tubes" conducted by Korkolis et al. and accept their conclusion that failure stresses become path-dependent if the pre-strain is significant. The reference paper has been added in the introduction paragraph 2 and section 4.3 paragraph 2 of the revised manuscript as reference [7].

In order to compare the difference in the amount of stress at the point of failure in bulging with stepped-dies and bulging with elliptical dies, the fracture stresses obtained from bulging with elliptical dies have been added to Fig. 11.

It can be found that the fracture stresses of $S_{1-0.4}^{0.1,R}$, $S_{1-0.6}^{0.1,R}$, $S_{1-0.4}^{0.1,T}$, $S_{1-0.6}^{0.1,T}$ and $S_{1-0.6}^{0.2,T}$ are in good agreement with the fracture stress curve obtained from bulging with elliptical dies. Meanwhile, the fracture stresses of $S_{1-0.6}^{0.2,R}$ are apparently higher than the fracture stress curve from elliptical bulging. These phenomena demonstrate that fracture stresses are much less path-dependent than fracture strains, and the path dependence of fracture stresses will become apparent if the strain level in the previous deformation is significant. These results are consistent with the conclusions confirmed by Korkolis et al. [7].

In addition, the phenomena and comments above have been added to section 4.3 paragraph 2 of the revised manuscript.

5. In order to compare the dies used in this study more accurate, I think it is better if their dimensions and differences are summarized in a table.

Response:

Based on the reviewer's suggestion, the dimensions of the three stepped-dies used in this study have been added to section 3.3 Table 3 of the revised manuscript.

6. Please determine the reference of equations 1, 8 and 13.

Response:

Thank the reviewer for the valuable suggestion. Modifications and additions to the three equations have been made to the revised manuscript as follows:

(1) The original Eq. (1), the Laplace's equation, describes the relationship between the two principle stresses. In section 2.2.1 of the revised manuscript, the relationship is redefined according to the force equilibrium in ND of the infinitesimal element at the pole point, where the effect of thickness is considered. The new relationship has been given in Eq. (3).

(2) The original Eq. (8) has been renumbered as Eq. (9). The equation is derived according to the definition of true strain in ND, namely Eq. (8), which has been added in section 2.2.3 of the revised manuscript.

(3) The original Eq. (13) has been renumbered as Eq. (17). The reference papers of this equation have been added as references [43] and [45] in section 4.5 of the revised manuscript. We refer to the Eq. (19) in the reference [43] and the Eqs. 2·7 and 2·11 in the reference [45] as plastic work rate equivalence has been used in many other literatures.

7. What standard test did you use to perform the uniaxial tensile and anisotropic tests?

Response:

Thank the reviewer for the suggestion. In the current work, the uniaxial tensile tests were performed according to testing standard GB/T 228.1-2010. The anisotropic coefficients were calculated using the plastic strain data up to the true tension strain of 0.2 according to standard GB/T 5027-2016. The two standards have been added to section 3.1 paragraph 2 of the revised manuscript.

8. It is not clear how you used reference 13 in Section 4.1. please explain the relationship between your sentence "Five points including the pole point were selected to fit in both RD and TD to provide more representative data sets [13]." and reference 13.

Response:

We are very sorry for our mistake of the wrong reference paper. The reference has been

corrected to [40] in section 4.1 paragraph 1 of the revised manuscript with the reference content mentioned in section 5.2.2, paragraph 3 of the reference paper.

9. Please add the constants values of Equation 7 with fitting accuracy in a new table in section 4.1.

Response:

Based on the reviewer's suggestion, the constants' values of Eq. (7) and fitting accuracy, Sum of Squares for Error (SSE) and coefficient determination (R^2), at different bulging heights in experiment $S_{1-0.4}^{0.1,R}$ have been added in section 4.1 Table 4 of the revised manuscript. The results show that accurate curvature radii can be obtained through parabolic fitting with five points.

Responses to Reviewer 3:

1. Figure 1. A three step stepped-die is presented, but the papers deals only with two steps tests. An upward z-axis on the left and a downward z-axis on the right would help the reader to distinguish the two different orientation of the die. A cut view of the die would help the lector.

Response:

Thank the reviewer for the valuable comments. The schematic of the stepped-die has been modified to a two-step one, as shown in Fig.1 of the revised manuscript. In addition, the descriptions of Fig. 1 have also been modified in section 2.1.

2. Page 8, Eq 1-5. The hypothesizes leading to the equations should be recalled, particularly the opening diameter to sheet thickness aspect ratio D/t. You neglect here the out-of-plane stress P/2 but this quantity should increase with the reduction of the radius. It would be important to give comments on that point.

Response:

As the Reviewer has highlighted, the ratio D/t is important in sheet bulging tests. Based on the reference papers [36,37] a clarification was added in section 2.2.1 paragraph 2 of the revised manuscript. As long as a small ratio of thickness to diameter of the bulge die is satisfied, typically at values lower than 1/50, the out-of-plane stress (the normal stress) $p/2$ can be neglected.

3. Page 9. Saying that 'the more points used the more accurate' seems a light

argumentation regarding the number of points and the size of the interpolation window used for the interpolation of your polynomial function. In section 4.1, it appears that only 5 points are used, equally 3.44mm spaced, and ref 13 is given. But, from reviewer knowledge, this reference doesn't deal with this issue. It seems to the reviewer that it would be important to give some proof of the validity of this choice for any of the radii measured hereafter.

Response:

The authors accept the reviewer's suggestion of the light argumentation that 'the more points used the more accurate' in section 2.2.2, which has been deleted in the revised manuscript.

We are very sorry for our mistake of the wrong reference paper. The reference has been corrected to [40] in section 4.1 paragraph 1 of the revised manuscript with the reference content mentioned in section 5.2.2, paragraph 3 of the reference paper.

In order to prove the validity of the choice of number of points and initial distance between two adjacent points, the values of the constants of Eq. (7) and fitting accuracy such as Sum of Squares for Error (SSE) and coefficient determination (R^2) at different bulging heights for the experiment $S_{1-0.4}^{0.1,R}$ have been determined and added to section 4.1 Table 4 of the revised manuscript. The results show that accurate curvature radii can be obtained through parabolic fitting with five points.

4. Page 10. Authors use a rough estimation of the thickness strain from the outer measured membrane strain, using plastic iso-volume hypothesis and neglecting elastic end bending strains. A correct estimation of the elastic strains should be given. ISO standard recommends to check for the amount of bending strain in the case of small D/t ratio. This point requires comments from the authors.

Response:

Based on the reviewer's suggestion section 2.2.3 has been modified for a more accurate pole thickness in the revised manuscript. The plastic incompressible deformation is assumed, the elastic strains are neglected and the bending strains are considered. In order to calculate the bending strains and the strain in ND, Eqs. (11) and (12) are added in section 2.2.3. This enables a more accurate pole thickness to be calculated according to Eqs. (9)-(12).

The reason for neglecting the elastic strains has been added to section 2.2.3 paragraph 3. That is "The elastic strain can be neglected considering that the plastic flow stresses of commonly used metal materials are sufficiently small relative to their elastic modulus". In addition, elastic strains for sheet bulging tests have been neglected in the literature [11], [18],

[19] and [21] cited in the revised manuscript. Moreover, the usage of neglecting the elastic strains is addressed in the standard ISO 16808: 2014. Therefore, we believe that it is reasonable to ignore the elastic strains.

5. Page 11. The pixel size should be given in mm/pixel.

Response:

Based on the reviewer's suggestion the description of the CCD cameras has been rewritten and the macro objective size monitored by the cameras has been added in section 3.2 paragraph 1 of the revised manuscript.

6. Page 13. How do the author select the initial radius of the first step? Do they use a numerical simulation? How this initial choice would affect the results for another material, another thickness? In other words, is the actual stepped die usable for another material, another thickness?

Response:

The reviewer's comments have been clarified in the revised manuscript as follows:

(1) The descriptions of the design method for the three stepped-dies has been rewritten in section 3.3 of the revised manuscript. The design of the die $S^{0.1}_{1-0.4}$ has been added as an example to section 3.3 paragraph 2.

The initial radius of the first step is designed to equal the curvature radius in RD at the pole point when ε_{RD}=0.1 (or 0.2) during bulging experiment with the circular die (E_1 in Fig.5). The position of the sphere is constrained tangentially by the fillet radii R_1=8 mm, which is the same as the circular die.

(2) The applicability of the new method to other materials has been added in section 4.6 paragraph 1 of the revised manuscript, namely: "The new method, bulging with stepped-dies, is developed based on the traditional bulging test method. Therefore, the new method is also usable for materials that can be tested using traditional bulging test method, such as steel, Aluminum alloy, Magnesium alloy and Titanium alloy [15,16,21]".

It should be noted that a small ratio of thickness to diameter of the bulge die is required, typically at values lower than 1/50, according to the reference paper [36,37] which have been added in section 2.2.1 paragraph 2.

7. In section 4.1 and 4.2, there is no new results compared to literature. The paragraph discussing the various evolutions of \gamma depending on the initial orientation of the RD is only a consequence of the choice made by the authors defining \lambda=Db/Da as a tool oriented value and \gamma=\rho_TD / \rho_RD as a material oriented one. This choice is not

questionable in itself, but the respective evolution of \gamma as a function of the initial orientation of the RD from major axis is just a consequence of this choice. Moreover it would have been interesting to compare the evolution of \gamma and 1/\gamma for S0.1T and S01R tests for example.

Response:

Thank the reviewer for the comments and suggestions. There are indeed many results about the curvature radii and thickness of traditional bulging tests in the literature. However, the results obtained from the new method by bulging with stepped-dies have not been published and the curvature radii and thickness during bulging tests are necessary for calculating the stress components. Therefore, we believe the results regarding the curvature radii and thickness should be given and discussed.

We accept the reviewer's opinion that the respective evolution of $\gamma=\rho_{TD}/\rho_{TD}$ as a function of the initial orientation of the RD from major axis is a consequence of the definition $\lambda=D_b/D_a$ in the original manuscript. In order to directly analyze the relationship between curvature radii and elliptical ratio λ, a new γ defined as the minor to major curvature radius ratio has been used in section 4.1 paragraph 5 of the revised manuscript.

Based on the Reviewer's suggestion, the evolutions of the minor to major curvature radius ratio γ during bulging with different dies have been added to section 4.1 Fig.8 of the revised manuscript. Through Fig. 8 the two curves obtained from the two bulging experiments can be compared with the same stepped-die but different specimen positions. It is found that the curves obtained from the same stepped-die but different specimen positions are almost identical. This result has been added to section 4.1 paragraph 5 of the revised manuscript.

8. Section 4.2. Line 6. What exactly is the end of the test? Onset of necking or fracture?

Response:

Thank the reviewer for the valuable comment. The end of the test is fracture. The last point on the curve in Fig. 9 (the original Fig. 8) is obtained from the last recorded image before fracture. In order to explain the end of the test clearly, we have added descriptions to section 4.2 of the revised manuscript, such as: "up to fracture" in line 1 of paragraph 1, and "obtained from the last recorded image before fracture" in line 4-5 of paragraph 2.

9. The calculation of the thickness is performed without any consideration for elastic and bending strain. This should be discussed in this section.

Response:

Based on the reviewer's suggestion section 2.2.3 has been modified for a more accurate

pole thickness in the revised manuscript. The plastic incompressible deformation is assumed, the elastic strains are neglected and the bending strains are considered. In order to calculate the bending strains and the strain in ND, Eqs. (11) and (12) are added in section 2.2.3. This enables a more accurate pole thickness to be calculated according to Eqs. (9)-(12).

The thicknesses shown in Fig. 9 of section 4.2 have been recalculated according to Eqs. (9)-(12) in section 2.2.3, and therefore, the calculation of the thickness is performed considering the bending strains.

In addition, the reason for neglecting the elastic strains has been added to section 2.2.3 paragraph 3. That is "The elastic strain can be neglected considering that the plastic flow stresses of commonly used metal materials are sufficiently small relative to their elastic modulus.".

10. Figure 12. A plot of the full path of one of the monotonous elliptical test would be worth plotting for comparison purpose.

Response:

Thank the reviewer for the valuable suggestion. The full strain paths of bulging experiments $E_{0.4}^{R}$ and $E_{0.4}^{T}$ have been added in Fig. 13 (the original Fig. 12). It can be found that the strain paths from bulging with elliptical dies are approximately linear over a wide range of deformations. All strain paths in Fig. 13 tend to the plane strain state at the end. These descriptions have been added in section 4.4 paragraph 1 and 2 with red color.

11. Figure 13. The respective effects of elastic and bending strains should be considered in the calculation of the behavior from experimental measurement on such small opening diameter to thickness ratios. For example, in the case S0.1R_1-0.4 it seems that the radius Rb is 20 mm only while the current thickness is about 0.68exp(-0.2)=0.56mm. So the D/t ratio is about 70 only.

Response:

Thank the reviewer for the suggestions. Section 2.2.1 has been modified and a model for stress components considering the effect of pole thickness has been provided in the revised manuscript. Meanwhile, more accurate equations for pole thickness have been added to section 2.2.3 in the revised manuscript. The plastic incompressible deformation is assumed, the elastic strains are neglected and the bending strains are considered with Eq. (11) used for the bending strains.

The equivalent stress-strain curves shown in Fig. 14 (the original Fig. 13) have been recalculated according to the new theoretical model of section 2.2, where the effect of thickness and the bending strains are considered.

In addition, the reason for neglecting the elastic strains has been added to section 2.2.3 paragraph 3. That is "The elastic strain can be neglected considering that the plastic flow stresses of commonly used metal materials are sufficiently small relative to their elastic modulus.".

12. Page 24. Last line. The 0.5 and 2 limit values are only theoretical values. This point should be recalled, and practical limit values should be given.

Response:

The authors agree with the reviewer's opinion that the 0.5 and 2 limit values are only theoretical values. It should be noted that the practical limit values of stress states that the bulge test can reach are related to the thickness of the sheet and the size of the die. It is difficult to give an exact limit without these data.

To explain the practical limit values that the bulge test can reach, a new paragraph has been added to the last of section 4.3 of the revised manuscript. That is:

"In order to achieve a plane strain condition a small λ should be used. This results in a large die being required to guarantee the small ratio of thickness to diameter. However, the size of the die is limited by experimental equipment constraints. Practically, Lenzen et al. [20,41] realized the condition of near plane strain through bulge test with an elliptical die of λ=0.375, and used the plane strain results as additional input data for material modelling."

Once again, we deeply appreciate editors and reviewers for their time and great efforts that help us improve our manuscript.

Highlights：

- A new concept of stepped-die with changing cross section shape is proposed
- Continuous nonlinear loading paths can be realized via bulging with stepped-dies
- Both stress and strain data of the whole process can be obtained during bulging
- The stress ratio changes from 0.5 up to 2.0 at most in one bulging experiment

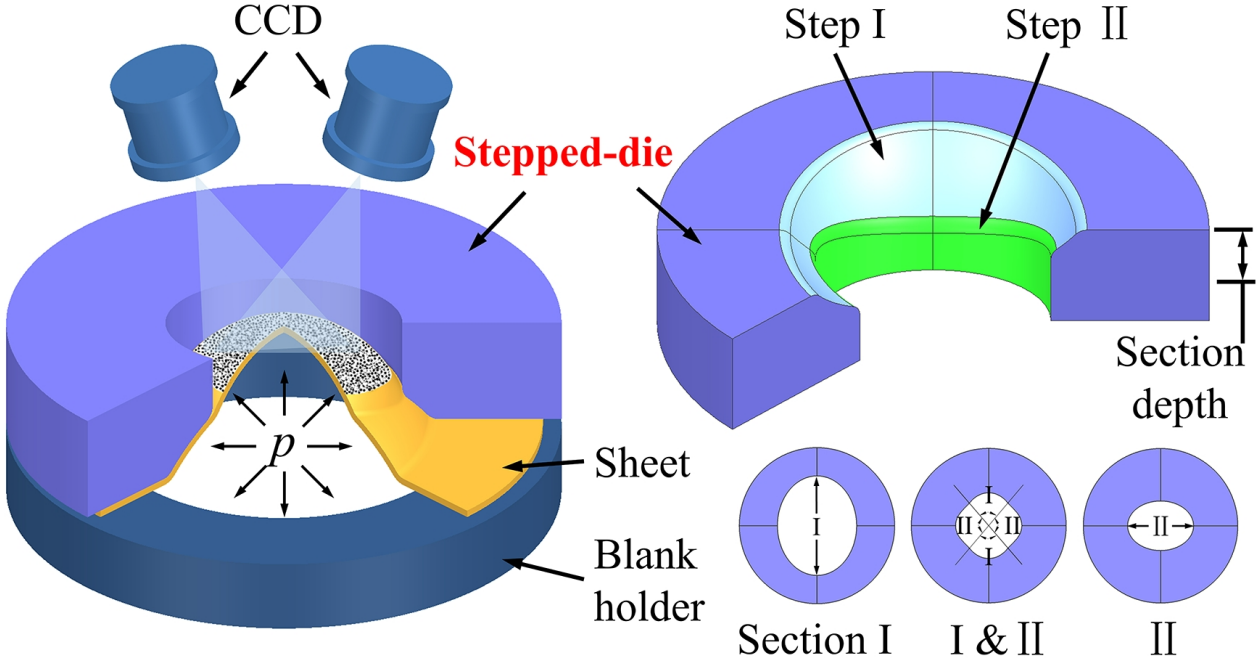

Principle of bulging with stepped-dies

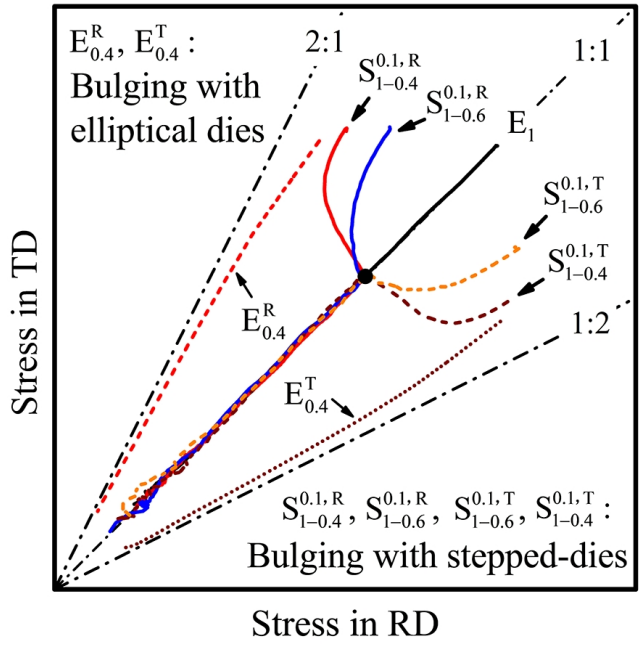

Stress paths from bulging tests

A novel test method for continuous nonlinear biaxial tensile deformation of sheet metals by bulging with stepped-dies

Zhubin He [a, b, *], Haihui Zhu [a], Yanli Lin [b], Denis J. Politis [c], Liliang Wang [c], Shijian Yuan [a]

[a] School of Materials Science & Engineering, Harbin Institute of Technology, Harbin 150001, P.R.China

[b] School of Mechanical Engineering, Dalian University of Technology, Dalian 116024, P.R.China

[c] Department of Mechanical Engineering, Imperial College London, London SW7 2AZ, UK

Corresponding author: Zhubin He

Postal address: School of Mechanical Engineering, Dalian University of Technology, 2 Linggong Road, Ganjingzi District, Dalian, 116024, P.R.China

E-mail address: hithe@hit.edu.cn

Telephone: +86-15244629678

Declarations of interest: none.

Abstract

In this paper, a novel test method named bulging with stepped-dies is proposed to overcome the difficulty of traditional test methods in realizing continuous nonlinear loading paths from initial yield up to fracture on a sheet metal. To achieve this aim, the section shape of a stepped-die cavity is varied with increasing depth. During bulging with a stepped-die, the stress state at the pole of bulging area of the sheet changes continuously with the increase in bulging height, which results in a specific nonlinear loading path. A theoretical model is established to calculate the stress components at the pole based on the assumption that the bulged surface near the pole was approximated by a rotational ellipsoid. Bulging experiments with three different stepped-dies are performed by using ST16 steel sheet. Stress and strain paths up to fracture and equivalent stress-strain curves at the pole are analyzed and compared with the results of bulging with elliptical dies. It is shown that continuous nonlinear loading paths can be effectively realized through bulging with stepped-dies and the stress ratio at the pole changes from 0.5 up to 2.0 at most in one bulging experiment. The feasibility of the novel test method is validated successfully. And the experimental data obtained are useful to determine constitutive and forming limit models suitable for complex loading conditions.

Keywords: nonlinear loading; biaxial tensile; stepped-die; bulge test; forming limit

1. Introduction

In sheet metal forming processes, metal sheets are subjected to various biaxial stress states. Testing and characterization of the mechanical behavior under the biaxial loading state have been key in the field of experimental plasticity. And one of the most important tasks is to improve the predictive accuracy of defect formations, such as springback and fracture [1].

Many anisotropic hardening behaviors have been observed under nonlinear loading conditions [2,3]. Path dependency of the forming limit has also been validated by multiple experimental studies [4-7]. Therefore, the material behavior under nonlinear loading paths cannot be evaluated comprehensively by using constitutive and forming limit models determined under linear loading paths. In order to determine the constitutive models and forming limit models under continuous nonlinear loading paths, an experimental method for continuous nonlinear biaxial tensile deformation of sheet metals is required.

In recent decades, several experimental methods for biaxial tests have been developed. One of the popular methods is the bulge test with circular or elliptical dies, which offers the advantage of absence of friction [8,9]. Bulging with a circular die is commonly used for determining the flow stress curves of sheet metals under biaxial tension [10,11], and it is also applied successfully to two-layer Al-Cu sheets [12]. Bulging test results under biaxial loading show that flow stress properties at higher strain levels could be obtained as compared to those obtained from uniaxial tensile tests, which is helpful for finite element simulation of severe plastic deformation [13].

Through bulging with different elliptical dies, the forming limit curve (FLC) can be evaluated [14-16], and the flow stress at the pole of the bulging area can be calculated by using theoretical model [17-19]. Lăzărescu et al. [18,19] developed an analytical model under the assumption that the bulged surface of the specimen is approximated to a rotational ellipsoid,

and determined the equivalent stress-strain curves. Moreover, Lenzen et al. [20] and Williams et al. [21] applied the stress state obtained from bulging with elliptical dies into the determination of yield surfaces. However, only linear or near-linear loading paths can be realized through bulge tests with circular or elliptical dies.

For investigating the effect of changing strain path on the FLC, Zhalehfar et al. [5] formed AA5083 under nonlinear loading paths through two-step dome test. The specimen used in the second step was prepared by cutting the specimen that had been stretched in the first step. Moreover, Sugawara et al. [22] developed a double-action punch stretching testing apparatus, the nonlinear strain paths of equal biaxial tension followed by plane-strain tension were realized without unloading.

In order to control or change the loading path continuously in one test, Kuwabara et al. [23-25] developed a biaxial tensile test method for sheet metals using a cruciform specimen. Nonlinear loading paths can be effectively realized through controlling the load on the four arms [26]. In order to observe high level of strains in the central region, a complex cruciform specimen with a reduced thickness in the central region must be designed [27-30]. As a result, biaxial tensile testing using a cruciform specimen is widely used to study yield and hardening behaviors of sheet metals.

To measure the deformation behavior of sheet metals under biaxial tension for a large strain range, Sumita et al. [31] and Kuwabara et al. [32] bent the sheet into a tubular specimen, and tested the tubular specimen by combining tension and internal pressure using a servo-controlled tube bulge testing machine developed by Kuwabara et al. [33,34]. The testing method is capable of measuring the elastic-plastic response of a tube to arbitrarily prescribed stress or strain paths from initial yield up to fracture [6,35]. However, the microstructure and mechanical properties of the tested sheet might be affected due to the bending process.

Therefore, in order to realize continuous nonlinear loading from the beginning of

deformation up to fracture, it is essential to develop a new test method for biaxial tensile deformation of sheet metals. As is well known, the stress ratio in bulging with an elliptical die depends on the elliptical ratio of the die. If bulging with a new die of which the elliptical ratio changes with the increase in cavity depth, the stress state will also change correspondingly. Thus, it is possible to obtain continuous nonlinear loading paths through bulging tests.

This paper aims to investigate the continuous nonlinear deformation of sheet metals using a novel test method. In section 2, the principle of bulging with stepped-dies and the theoretical model for calculating stress components are presented. In section 3, the experimental work is described, including the experimental set-up and experimental scheme involving three specifically designed stepped-dies, three elliptical dies and one circular die. In section 4, stress and strain paths up to fracture and equivalent stress-strain curves during bulging with three different stepped-dies are analyzed and compared with the results of bulging with elliptical dies. In addition, possible applications and future works of the new method are discussed.

2. Description of bulging with stepped-die

2.1. Principle

The principle of bulging with stepped-dies is shown in Fig. 1. The die is named as stepped-die in view of the characteristic of changing elliptical ratio. As shown in Fig. 1(a), the sheet is pressed over the stepped-die by the blank holder with the effect of preventing the pressed regions of the sheet from flowing into the die cavity. The free area of the sheet will be bulged gradually by the bulging pressure p until fracture occurs. Generally, fractures are located near the pole of the bulged specimens. Two CCD cameras are used for monitoring strains and displacements in real time based on the Digital Image Correlation (DIC) technology.

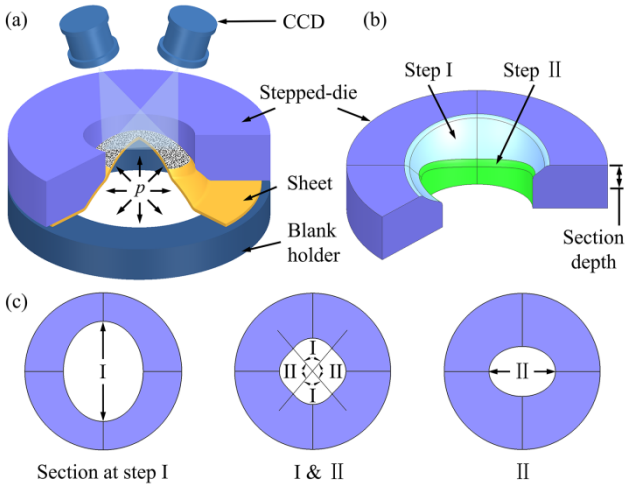

Fig. 1. Principle of bulging with stepped-dies: (a) schematic of bulging with stepped-dies, (b) schematic of a typical stepped-die, (c) sections of the typical stepped-die at different depths.

A typical stepped-die is shown in Fig. 1(b). The die cavity is divided into two steps, step I is a portion of a rotational ellipsoid, and step II is an elliptical hole. The two major axes in the two steps are perpendicular to each other. Fig. 1(c) shows three cross sections of the typical stepped-die at different depths. The size of cross section decreases with the increase of depth, and the shape of section changes from an elliptical in step I into another elliptical in step II. It is worth noting that a sphere is a special rotational ellipsoid. If the shape of step I is designed to a sphere, the deformation of the sheet will begin with equal biaxial tension.

For the bulging test shown in Fig. 1, the contact boundary of the bulging area is located at the entrance fillet of the die during step I. Once the sheet fully contacts the surface of step I, the contact boundary will rapidly turn into the elliptical hole in step II, or to say the fillet between step I and step II. At that moment, the stress state will change suddenly.

2.2 Theoretical model

2.2.1 Stress components

Rolled sheet metals are generally regarded as orthotropic materials, and their orthotropy axes are rolling direction (RD), transverse direction (TD) and normal direction (ND). The

geometry of the free region of the specimen during bulging with a stepped-die is shown schematically in Fig. 2. The three orthotropy axes RD, TD and ND of the specimen coincide with the axes *X*, *Y* and *Z*, respectively. The origin point O of the coordinate system is located at the center of the flat specimen. In the figure, *h* represents bulging height, *a* and *b* represent the width of contact boundary in RD and TD, respectively. It should be noted that the shape of the contact boundary and the values of *a* and *b* will change as the bulging height increases.

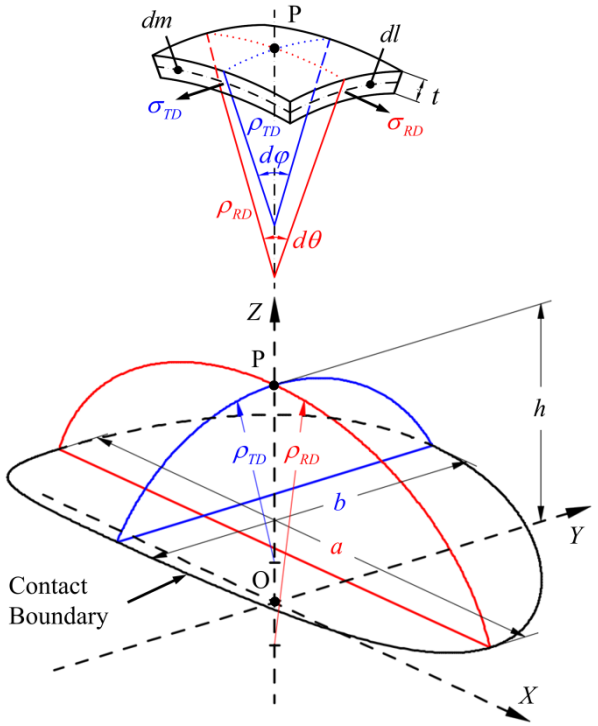

Fig. 2. Geometry of the free region of the specimen and stress analysis during bulging with a stepped-die.

Stress analysis of the sheet can be performed with the aid of the membrane theory, as long as a small ratio of thickness to diameter of the bulge die is satisfied, typically at values lower than 1/50 [36,37]. Under these conditions, the bending stress and the normal stress can be neglected resulting in the stress analysis of the infinitesimal element at the pole point P, as shown in Fig. 2.

Based on this infinitesimal element, the following assumptions are further made: (1) the thickness *t* is uniform; (2) the two principle stresses σ_{RD} in RD and σ_{TD} in TD are uniform

and normal to the corresponding section surfaces; and the outer curvature radii ρ_{RD} and ρ_{TD} are uniform over the infinitesimal element.

From the force equilibrium in ND, the following relationship can be obtained:

$$\begin{aligned} &2\sigma_{RD}\left(dl\cdot t\right)\sin(d\theta/2)+2\sigma_{TD}(dm\cdot t)\sin(d\varphi/2)\\ &=p\left[2\left(\rho_{RD}-t\right)\sin(d\theta/2)\cdot 2(\rho_{TD}-t)\sin(d\varphi/2)\right] \end{aligned} \tag{1}$$

Where p is the bulging pressure, dl and dm are the arc lengths along RD and TD at the neutral layer of the infinitesimal element. $d\theta$ and $d\varphi$ are the two small central angles of dl and dm, respectively. Therefore, $\sin(d\theta/2)$ and $\sin(d\varphi/2)$ can be reduced to:

$$\begin{cases} \sin(d\theta/2)=d\theta/2=\dfrac{dm}{2\rho_{RD}-t}\\ \sin(d\varphi/2)=d\varphi/2=\dfrac{dl}{2\rho_{TD}-t} \end{cases} \tag{2}$$

Thus, Eq. (1) can be re-written as:

$$\frac{\sigma_{RD}}{\rho_{RD}-t/2}+\frac{\sigma_{TD}}{\rho_{TD}-t/2}=\frac{p}{t}\frac{(\rho_{RD}-t)(\rho_{TD}-t)}{(\rho_{RD}-t/2)(\rho_{TD}-t/2)} \tag{3}$$

In many works, the profiles of specimens bulged with elliptical dies were approximated by rotational ellipsoids with the rotational axis parallel to the major axis of the die [18-20,38]. During bulging with elliptical dies, the curvature radii in the major axis are always greater than that in the minor axis. During bulging with stepped-dies, the relationship between ρ_{RD} and ρ_{TD} may change if the section shape of the die changes significantly.

Therefore, the profile near the pole point of the specimen bulged with a stepped-die should be approximated by a rotational ellipsoid with the rotational axis parallel to the direction of the larger one of ρ_{RD} and ρ_{TD}. For the condition $\rho_{RD}\geq\rho_{TD}$, the rotational axis of the ellipsoid should be parallel to RD, resulting in σ_{RD} being calculated using the following equation:

$$\sigma_{RD}=\frac{p\left(\rho_{TD}-t\right)}{2t} \tag{4}$$

By substituting Eq. (4) into Eq. (3), σ_{TD} can be obtained by:

$$\sigma_{TD} = \frac{p(\rho_{TD} - t)}{2t} \frac{2(\rho_{RD} - t) - (\rho_{TD} - t/2)}{(\rho_{RD} - t/2)} \tag{5}$$

Conversely, when $\rho_{RD} < \rho_{TD}$ the equations for σ_{RD} and σ_{TD} should be adjusted accordingly.

2.2.2 Curvature radius

In order to calculate the stress components it is necessary to measure the two curvature radii ρ_{RD} and ρ_{TD}. Parabolic fitting with a quadratic polynomial can be used to fit the profile of the bulged specimen [9,39]. Assuming that (X_1, Z_1) and (Y_2, Z_2) are coordinates of points on the outer surface of the specimen in the XOZ plane and the YOZ plane, respectively, the coordinates satisfy the following relationship:

$$\begin{cases} Z_1 = A_1 X_1^{\,2} + B_1 X_1 + C_1 \\ Z_2 = A_2 Y_2^{\,2} + B_2 Y_2 + C_2 \end{cases} \tag{6}$$

Where A_1, B_1, C_1 and A_2, B_2, C_2 are the coefficients of the two quadratic curves.

Thus, ρ_{RD} and ρ_{TD}. at the pole point P (X_P, Y_P, Z_P) can be expressed as follows:

$$\begin{cases} \rho_{RD} = \dfrac{\left[1 + (2A_1 X_P + B_1)^2\right]^{3/2}}{2|A_1|} \\ \rho_{TD} = \dfrac{\left[1 + (2A_2 Y_P + B_2)^2\right]^{3/2}}{2|A_2|} \end{cases} \tag{7}$$

The three coefficients of each quadratic curve can be solved analytically when coordinates of three points on the curve are known. However, it is believed that using three points might lead to erroneous results due to possible local imperfections. If coordinates of more than three points are utilized, these coefficients can be obtained by parabolic fitting based on the least square method.

2.2.3 Pole thickness

According to the definition of true strain, the strain in ND at the pole point can be expressed as:

$$\varepsilon_{ND} = \ln\left(t/t_0\right) \tag{8}$$

Where t_0 is the initial thickness of the specimen. Therefore, the actual thickness t at the pole point during bulging can be calculated by:

$$t = t_0 \exp\left(\varepsilon_{ND}\right) \tag{9}$$

The elastic strain can be neglected considering that the plastic flow stresses of commonly used metal materials are sufficiently small relative to their elastic modulus. Assuming plastic incompressible deformation of the sheet metal and ignoring the elastic strains and the influence of bending, the strain in ND can be approximated by:

$$\varepsilon_{ND} \approx -\varepsilon_{RD} - \varepsilon_{TD} \tag{10}$$

Where, the principle strains ε_{RD} and ε_{TD} of outer surface in RD and TD at the pole point can be measured by DIC.

It should be noted that the influence of bending could be ignored only when the ratio of thickness to die diameter is reasonably small to ensure a near membrane stress state in the test sheet. For thickness to die diameter ratios greater than 1/100, the bending strain can be calculated using the standard ISO 16808 [9] with the equation:

$$\varepsilon^b = -\ln\left[1 - \frac{t_0 \exp\left(-\varepsilon_{RD} - \varepsilon_{TD}\right)}{2\rho}\right] \tag{11}$$

Where, ε^b and ρ are the bending strain and curvature radius of outer surface in RD or TD at the pole point. Then, a more accurate formulation for the strain in ND can be obtained with the equation:

$$\varepsilon_{ND} = -\left(\varepsilon_{RD} - \varepsilon_{RD}^b\right) - \left(\varepsilon_{TD} - \varepsilon_{TD}^b\right) \tag{12}$$

3. Experimental work

3.1 Material

A low carbon deep drawing steel sheet ST16 with a nominal thickness of 0.68mm, mostly used for automotive components and body panels, was chosen for the experiments in this work. The chemical compositions of ST16 are summarized in Table 1.

Table 1. Chemical compositions of ST16 (wt%).

Element	C	Si	Mn	P	S	Als	Ti	Fe
Value	0.12	1.3	10	1.1	0.8	2.1	7.1	Bal.

Uniaxial tensile tests were performed in 0°, 45° and 90° angles measured from RD according to the standard GB/T 228.1-2010. The dimensions of the tensile test specimens and the true stress-strain curves of ST16 up to the diffuse necking are shown in Fig. 3. The mechanical properties of ST16 deduced from the tensile tests are shown in Table 2. The Lankford coefficients were calculated using the plastic strain data up to the true tensile strain of 0.2 according to the testing standard GB/T 5027-2016. The hardening parameters were fitted by using the true stress-strain data at 0° based on the hardening model $\sigma = K\varepsilon^n$.

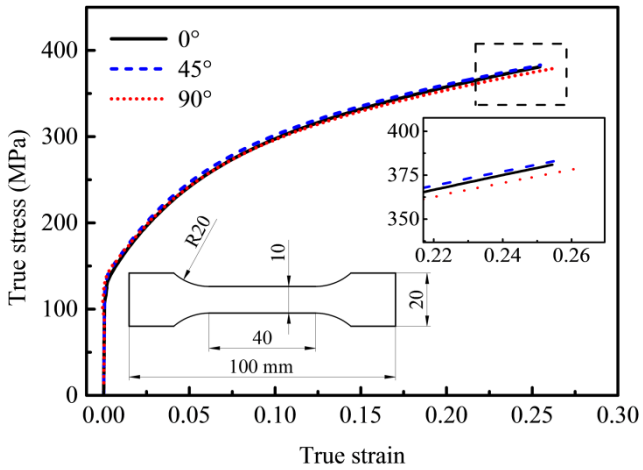

Fig. 3. Dimensions of specimen and true stress-strain curves of ST16 up to diffuse necking.

Table 2. Mechanical properties of ST16 obtained by uniaxial tensile test.

Properties	0°	45°	90°
Yield stress, σ_s (MPa)	135.5	141.3	137.5
Ultimate tensile strength, σ_{uts} (MPa)	295.6	297.2	291.6
Lankford coefficient, r	1.942	2.193	2.699
Hardening coefficient, K (MPa)	554.7	551.1	543
Strain-hardening exponent, n	0.271	0.262	0.265

It can be seen from Fig. 3 that the true stress-strain curves at 0°, 45° and 90° are almost identical. Moreover, all the Lankford coefficients listed in Table 2 are greater than 1, and r_{90} surpass r_0 by 39%. This demonstrates that ST16 steel sheet has obvious anisotropy both in the thickness direction and in plane.

3.2 Experimental set-up

The experimental set-up shown in Fig. 4 was used to perform bulging experiments with stepped-dies. The experimental set-up consists of a stepped-die, a 50-ton cylinder for maintaining the blank holder force, a hydraulic device for developing the bulging pressure p, a pressure transducer with measurements ranging from 0 to 40MPa, and a DIC system with two CCD cameras, XTDIC 3D full-field strain measurement and analysis system developed by Xi'an Jiaotong University. Each camera is equipped with a 1628×1236 pixel^2 sensor. The strain and displacement measurement accuracy of XTDIC are 0.005% and 0.01 pixel, respectively. In this work the macro objective added to the camera was about 138×105 mm.

The cameras were positioned to record the specimen deformation via a circular hole of 120 mm diameter located in the center of the upper beam. The speckle pattern painted on the outer surface of the specimen was recorded by CCD cameras through the hole. In order to protect the CCD cameras from potential damage, a transparent glass plate was placed between the cameras and the upper beam.

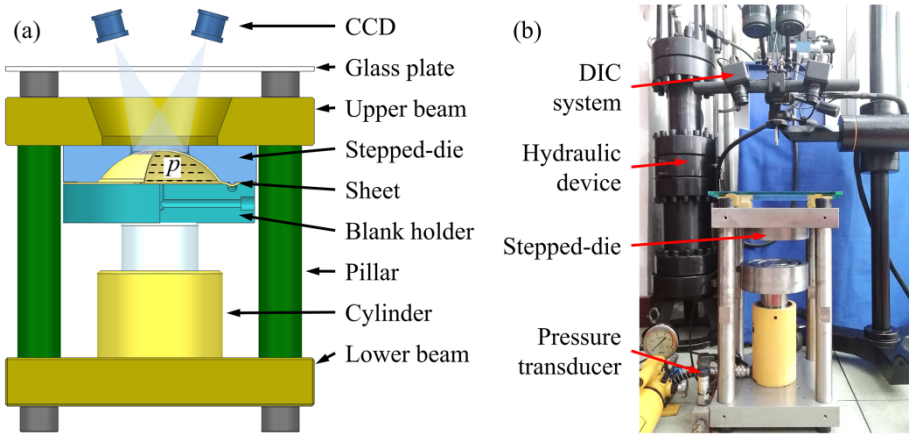

Fig. 4. Experimental set-up: (a) schematic diagram and (b) physical image.

3.3 Experimental scheme

For validating the feasibility of the test method by bulging with stepped-dies, three stepped-dies ($S^{0.1}_{1-0.4}$, $S^{0.1}_{1-0.6}$ and $S^{0.2}_{1-0.6}$) with two steps were designed based on a typical loading path, i.e. an equal biaxial tension followed by unequal biaxial tension, as shown in Fig. 5. Step I is a portion of a sphere with radius *SR* whereas Step II is an elliptical hole. The fillet radii are R_1=8 mm and R_2=5 mm in the three stepped-dies. The elliptical ratio λ can be defined as the ratio of the minor axis length D_b and major axis length D_a:

$$\lambda = D_b / D_a \tag{13}$$

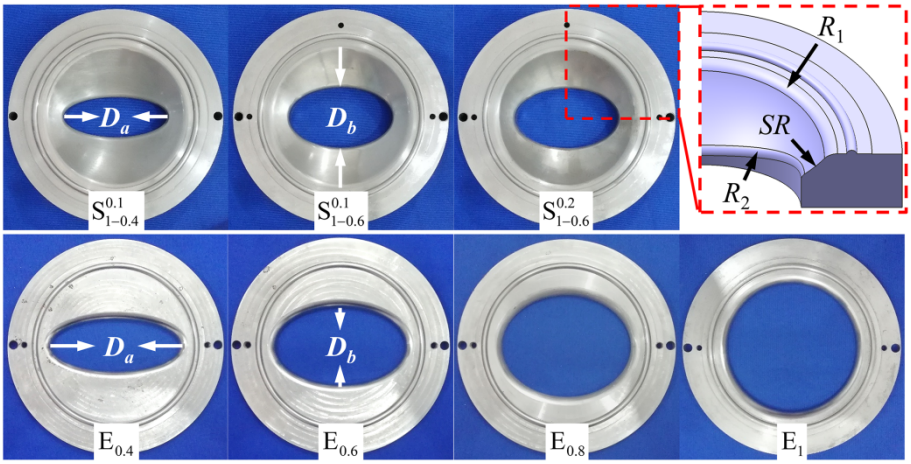

Fig. 5. Images of the stepped-dies, the elliptical dies and the circular die.

Detailed information of the three stepped-dies is summarized in Table 3. By taking $S^{0.1}_{1-0.4}$

as an example, the superscript 0.1represents ε_{RD}=0.1 at the pole point at the end of step I. For this purpose, the radius of sphere *SR* in step I is designed to be 97.6 mm, corresponding to the curvature radius ρ_{RD} when ε_{RD}=0.1 in the bulging test with the circular die E_1 (shown in Fig. 5). And the position of the sphere is constrained tangentially by the fillet R_1, which is the same as the fillet of die E_1. The subscript 1-0.4 means that λ changes from 1 in step I to 0.4 in step II. In addition, the radius of sphere *SR* of die $S_{1-0.4}^{0.2}$ is equal to ρ_{RD}=76.3 mm when ε_{RD} =0.2 in the bulging test with the circular die E_1.

Table 3. Dimensions of the three stepped-dies.

Die number	step I			step II	
	D_a (mm)	λ	Strain level	D_a (mm)	λ
$S_{1-0.4}^{0.1}$	120	1	ε_{RD}=0.1	100	0.4
$S_{1-0.6}^{0.1}$	120	1	ε_{RD}=0.1	100	0.6
$S_{1-0.6}^{0.2}$	120	1	ε_{RD}=0.2	100	0.6

In order to analyze the relationship and difference between the bulging with stepped-dies and bulging with elliptical dies, elliptical and circular dies ($E_{0.4}$, $E_{0.6}$, $E_{0.8}$ and E_1) with λ =0.4, 0.6, 0.8 and 1 were designed, as shown in Fig. 5. The major axis length was D_a=120 mm and the fillet radius was 8 mm in the four dies.

It should be noted that different results may be obtained depending on specimen positions relative to the bulging die due to anisotropy of the specimens. Two different specimen positions, RD in the major axis of the die and TD in the major axis of the die, were applied. When bulging with RD (TD) in the major axis, the experiment number was marked with a superscript letter R (T) on the die number, for example, $S_{1-0.4}^{0.1,R}$ and $E_{0.4}^{T}$.

4. Results and discussions

The bulged specimens are shown in Fig. 6. It can be seen that the shapes of specimens bulged with stepped-dies consist of two parts corresponding to the two steps of the dies.

Fractures are located near the pole and parallel to the major axis of the elliptical hole in step II. Similar fractures were found in bulging with elliptical dies. Specifically, the fracture was inclined at approximately 18° to RD in the specimen bulged with the circular die E_1.

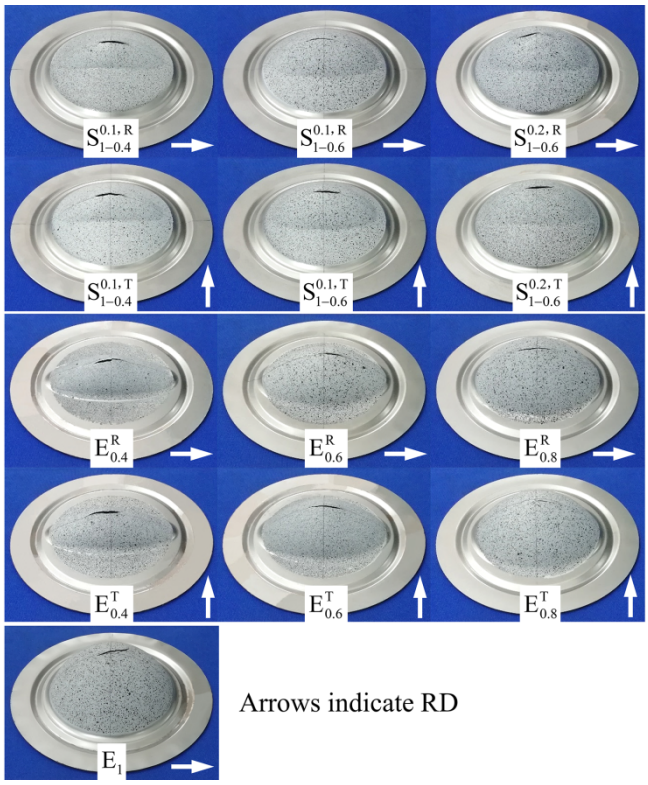

Fig. 6. Images of bulged specimens.

4.1 Curvature radii

The two curvature radii ρ_{RD} and ρ_{TD} at the pole point during bulging were fitted based on the least square method introduced in section 2.2.2. Five points including the pole point were selected to fit in both RD and TD to provide more representative data sets [40]. The initial distance between two adjacent points was 3.44 mm.

The values of the constants of Eq. (7) and fitting accuracy such as Sum of Squares for Error (SSE) and coefficient determination (R^2) at different bulging heights for the experiment $S_{1-0.4}^{0.1,R}$ are listed in Table 4. The results show that accurate curvature radii can be obtained through parabolic fitting with five points.

Table 4. The constants values of Eq. (7) and fitting accuracy, SSE and R^2, in experiment $S_{1-0.4}^{0.1,R}$.

h (mm)	A_1	B_1	SSE	R^2	A_2	B_2	SSE	R^2
5	-1.2×10^{-3}	-7.4×10^{-4}	6.2×10^{-5}	0.9803	-1.3×10^{-3}	-6.9×10^{-4}	3.2×10^{-5}	0.9901
10	-2.0×10^{-3}	-1.1×10^{-3}	1.1×10^{-5}	0.9987	-2.0×10^{-3}	-2.2×10^{-4}	3.1×10^{-6}	0.9996
24.8	-5.2×10^{-3}	-2.9×10^{-4}	5.6×10^{-5}	1	-5.6×10^{-3}	1.2×10^{-3}	3.5×10^{-5}	0.9996
34.2	-9.0×10^{-3}	4.0×10^{-3}	2.7×10^{-4}	0.9993	-2.1×10^{-2}	9.8×10^{-3}	1.9×10^{-4}	0.9999

Fig. 7 shows curvature radius ρ_{RD} as a function of bulging height h from bulging with stepped-dies. Points A and B correspond to the two states of ε_{RD}=0.1 and ε_{RD}=0.2 in bulging with E_1, as well as the two transition points from step I to step II in bulging with stepped-dies. Curves obtained from bulging with stepped-dies coincide with the curve E_1 before the transition points A or B, because the contact boundary in step I is the same as bulging with E_1.. At the points A or B, the surface of the specimen is attached to the sphere of the stepped-die. Afterwards, the free region of the specimen is bulged under the constraint from the hole in step II and the fillet R_2. As a result, curves obtained from bulging with stepped-dies transit away from the curve E_1.

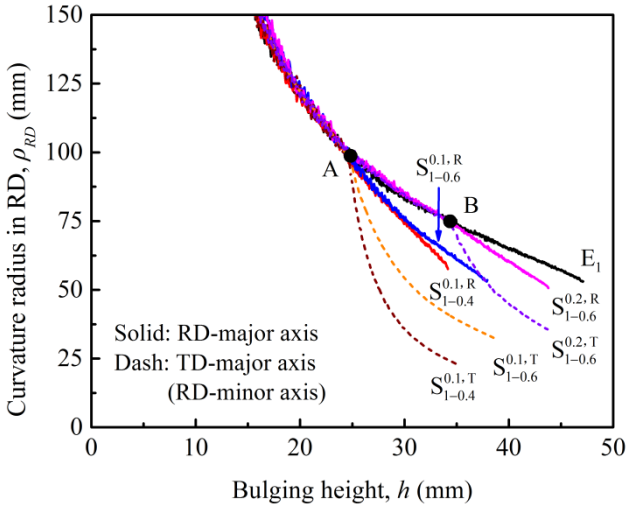

Fig. 7. Curvature radius in RD vs bulging height from bulging with stepped-dies.

It can be seen in Fig. 7 that ρ_{RD} decreases with the increase of h. After crossing the points A or B, ρ_{RD} decreases at a higher rate. Moreover, the curvature radii in the minor axis

direction decrease faster than the curvature radii in the major axis direction. Comparing the curves $S_{1-0.4}^{0.1,R}$ with $S_{1-0.6}^{0.1,R}$, it can be found that after being bulged with the same sphere in step I, ρ_{RD} in $S_{1-0.4}^{0.1,R}$ is smaller than ρ_{RD} in $S_{1-0.6}^{0.1,R}$ at the same bulging height even though the widths of the major axis of the elliptical hole D_a are the same. This phenomenon indicates that the curvature radius at the pole is not just dependent on the width and height of the profile along the corresponding direction, and that there is a coupling relationship between the two curvature radii.

Fig. 8 shows the relationship between the minor to major curvature radius ratio γ and bulging height h in bulging with stepped-dies. $\gamma = \rho_{TD}/\rho_{RD}$ when the specimen position is RD in the major axis and $\gamma = \rho_{RD}/\rho_{TD}$ when TD is in the major axis. It can be found that the curves obtained from the same stepped-die although at different specimen positions are almost identical. Moreover, the value of γ decreases towards λ during step II. For example, the curves $S_{1-0.4}^{0.1,R}$ decreases towards 0.4. These phenomena were also observed in bulging with elliptical dies. The reason is that if the specimen could be bulged sufficiently, the curvature radius in the major (minor) axis will equal to half the length of the major (minor) axis of the die.

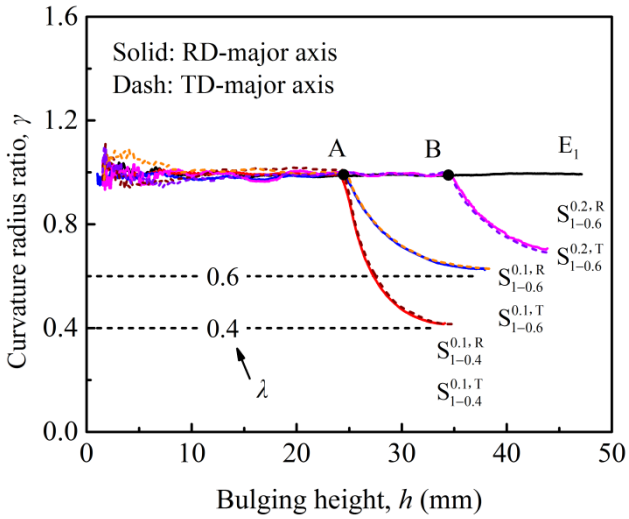

Fig. 8. Minor to major curvature radius ratio vs bulging height from bulging with stepped-dies.

4.2 Thicknesses

Fig. 9 shows curves of pole thickness t up to fracture, calculated according to Eqs. (9)-(12) from bulging with stepped-dies. Once crossing the points A or B, the curves obtained from bulging with stepped-dies decrease rapidly.

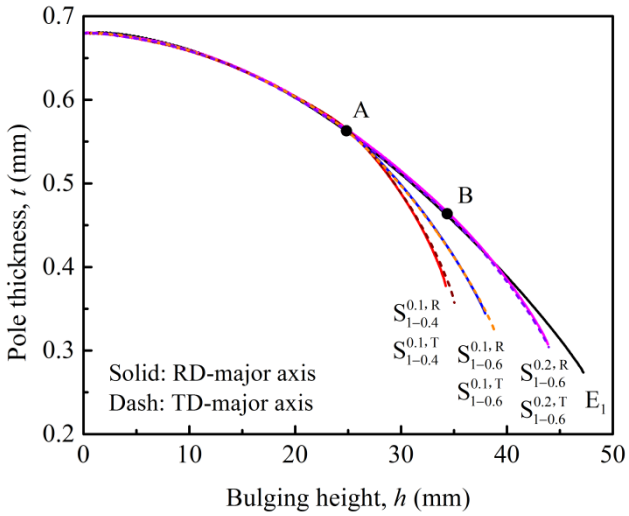

Fig. 9. Pole thickness vs bulging height from bulging with stepped-dies.

Comparing curves $S_{1-0.4}^{0.1,R}$ with $S_{1-0.6}^{0.1,R}$ in Fig. 9, it can be found that after being bulged with the same sphere in step I, the smaller the value of λ in step II the faster the thickness decreases. Moreover, comparing the curves $S_{1-0.6}^{0.1,R}$ with $S_{1-0.6}^{0.2,R}$, it can be found that when the pole strain in RD at the end of step I increases from 0.1 to 0.2, the final pole thickness obtained from the last recorded image before fracture decreases from 0.345 to 0.307 mm. The two curves obtained from the same die but at different specimen positions follow the same rule, although thinner final pole thicknesses were obtained from bulging with TD in the major axis.

Distributions of thickness thinning, the negative of Eq. (10), on the deformed specimens $S_{1-0.4}^{0.1,R}$, $S_{1-0.6}^{0.1,R}$ and $S_{1-0.6}^{0.2,R}$ at different bulging heights were analyzed through DIC, as shown in Fig. 10. Taking Fig. 10(a) as an example, at the end of step I the contour lines were approximately circular, and the center was located at the pole. During step II, the shape of the

contour lines gradually shifted to elliptical, and the directions of the major and minor axes were the same as those of the elliptical hole. During the whole bulging process, the area of greatest thinning was always near the pole, indicating the location of the fracture. These phenomena were also observed in other bulging experiments with stepped-dies.

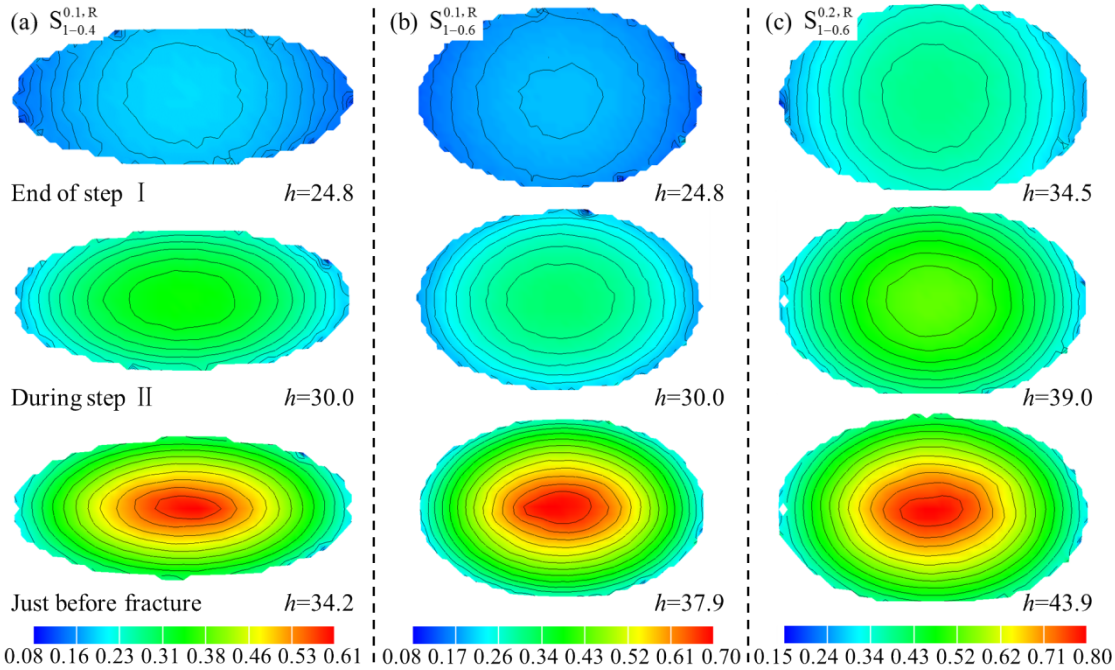

Fig. 10. Thickness thinning at different bulging heights in (a) $S_{1-0.4}^{0.1,R}$, (b) $S_{1-0.6}^{0.1,R}$ and (c) $S_{1-0.6}^{0.2,R}$.

4.3 Stress paths and fracture stresses

The stress paths up to fracture from bulging with different dies are shown in Fig. 11. It is found that the stress paths from bulging with stepped-dies were distinctly nonlinear. In addition, the curve $S_{1-0.4}^{0.1,R}$ with λ=0.4 was observed to exhibit a sharper change than the curve $S_{1-0.6}^{0.1,R}$ with λ=0.6. More importantly, the stress path from bulging with a stepped-die changed towards the path from bulging with an elliptical die, when the two dies had the same elliptical ratio. For example, the curve $S_{1-0.4}^{0.1,R}$ changes towards the curve $E_{0.4}^{R}$, when both the elliptical ratios are 0.4.

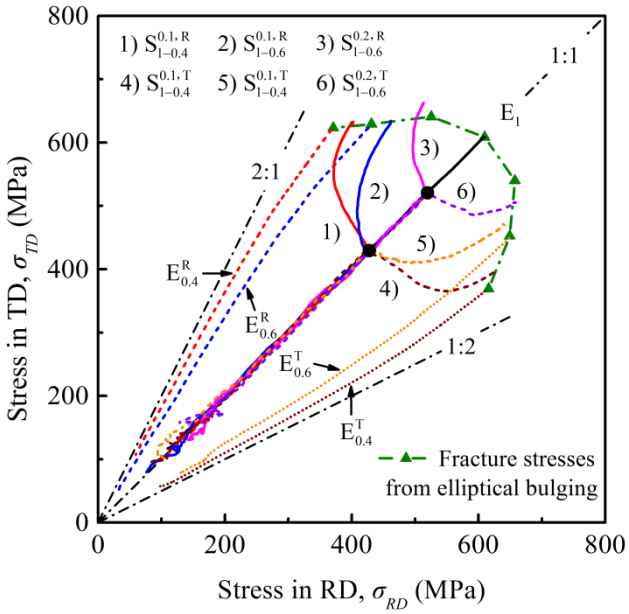

Fig. 11. Stress paths from bulging with different dies and fracture stresses from bulging with elliptical dies.

In Fig. 11 it can be also found that the fracture stresses of $S^{0.1,R}_{1-0.4}$, $S^{0.1,R}_{1-0.6}$, $S^{0.1,T}_{1-0.4}$, $S^{0.1,T}_{1-0.6}$ and $S^{0.2,T}_{1-0.6}$ are in good agreement with the fracture stress curves obtained from bulging with elliptical dies. Meanwhile the fracture stresses of $S^{0.2,R}_{1-0.6}$ are apparently greater than the fracture stress curve from elliptical bulging. These phenomena demonstrate that fracture stresses are much less path-dependent than fracture strains, and the path dependence of fracture stresses will become apparent if the strain level in the previous deformation is significant. These results are consistent with the conclusions confirmed by Korkolis et al. [7].

The results of the stress ratio $\alpha = \sigma_{TD}/\sigma_{RD}$ as a function of bulging height h from bulging with stepped-dies are shown in Fig. 12. It can be seen that the stress ratio changes towards a constant with the increase of bulging height. The constant equals to 2-λ when the specimen position is RD in the major axis, or equals to 1/(2-λ) when the specimen position is TD in the major axis. For example, α in $S^{0.1,R}_{1-0.4}$ changes towards 1.6, and α in $S^{0.1,T}_{1-0.4}$ changes towards 0.625.

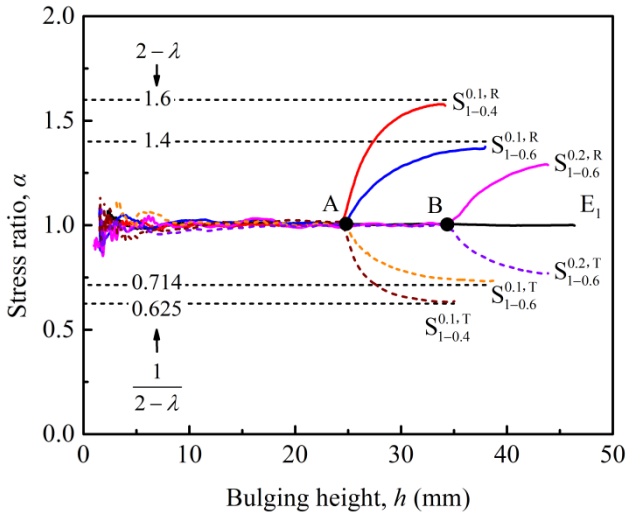

Fig. 12. Stress ratio vs bulging height from bulging with stepped-dies.

According to the analysis of stress paths and stress ratios, the nonlinear loading path obtained from bulging with a stepped-die is determined by the change of cross section of the die cavity for a given sheet metal and its position relative to the die. The greater the difference between the two sections, the greater the nonlinearity of the stress path. For example, if the stepped-die has a step III, another sudden change will occur when the bulging process changes from step II into step III. If the section shape of the stepped-die changes smoothly, the stress state will also change smoothly.

When the specimen is bulged in a narrow section with the limit $\lambda \to 0$, the limit $\alpha \to 2.0$ if the specimen position is RD in the major axis, or the limit $\alpha \to 0.5$ if the specimen position is TD in the major axis. The deformation type will be the plane strain state with the increment of the minor strain component equaling to 0. Consequently, the stress ratio at the pole can change from 0.5 up to 2.0 at most in one bulging experiment with a stepped-die, of which the initial cross section and the final cross section are perpendicular to each other and have the same $\lambda \to 0$.

In order to achieve the plane strain condition a small λ should be used. This results in a large die being required to guarantee the small ratio of thickness to diameter. However, the size

of the die is limited by experimental equipment constrains. Practically, Lenzen et al. [20,41] realized the condition of near plane strain through bulge test with an elliptical die, of which λ = 0.375, and used the plane strain results as additional input data for material modelling.

4.4 Strain paths and fracture strains

Strain paths from bulging with different dies and fracture strains from bulging with elliptical dies are shown in Fig. 13. The strain paths from bulging with elliptical dies such as $E_{0.4}^{R}$ are approximately linear over a wide range of deformations, whereas the strain paths from bulging with stepped-dies are clearly nonlinear. These curves gradually deviate from the state of equal biaxial tension during bulging in step II as shown with the curve $S_{1-0.4}^{0.1,R}$ at λ=0.4 which deviates faster than the curve $S_{1-0.6}^{0.1,R}$ with λ=0.6.

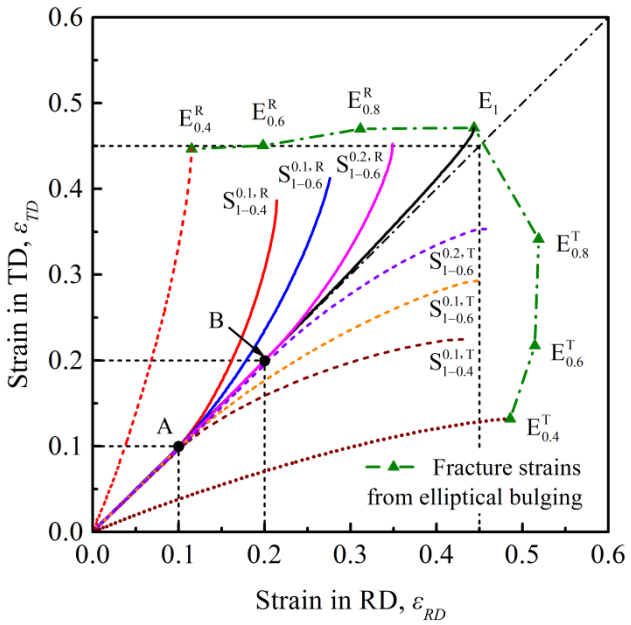

Fig. 13. Strain paths from bulging with different dies and fracture strains from bulging with elliptical dies.

All strain paths in Fig. 13 tend to the plane strain state or the state when the increment of the minor strain equals to 0 before fracture occurs. According to this phenomenon, Hora et al. [42,43] developed the Modified Maximum Force Criterion (MMFC) for the theoretical evaluation of FLC.

It should be noted in Fig. 13 that fracture strains from bulging with the three stepped-dies are obviously lower than fracture strains from bulging with elliptical dies. The difference illustrates the path-dependence of the forming limit strains in sheet metal forming. Moreover, strain paths from bulging with specimen position of RD in the major axis and that from bulging with TD in the major axis direction are almost symmetric along the diagonal. However, fracture strain points are not as symmetrical. Fracture strains in RD obtained from experiments with TD in major axes such as $E_{0.4}^{T}$ and $S_{1-0.4}^{0.1,T}$ are clearly greater than fracture strains in TD obtained from experiments with RD in the same major axes such as $E_{0.4}^{R}$ and $S_{1-0.4}^{0.1,R}$. The phenomenon is a result of the constitutive model and microstructure of the material which is beyond the scope of this study.

4.5 Equivalent stress-strain curves

The Barlat 1989 anisotropic yield criteria [44] is popularly used in finite element simulations of sheet metal forming, and can describe the yield locus of low carbon steels well. The Barlat 1989 yield criterion can be expressed as:

$$f = a\left|k_1 + k_2\right|^M + a\left|k_1 - k_2\right|^M + c\left|2k_2\right|^M = 2\bar{\sigma}^M \tag{14}$$

$$k_1 = \frac{\sigma_{xx} + h\sigma_{yy}}{2}; \quad k_2 = \left[\left(\frac{\sigma_{xx} - h\sigma_{yy}}{2}\right)^2 + q^2\sigma_{xy}^2\right]^{1/2} \tag{15}$$

Where M is an integer exponent, $M = 6$ for BCC materials and $M = 8$ for FCC materials. a, c, h and q are material constants:

$$\begin{aligned} a &= 2 - c = 2 - 2\sqrt{\frac{r_0}{1+r_0}\cdot\frac{r_{90}}{1+r_{90}}} \\ h &= \sqrt{\frac{r_0}{1+r_0}\cdot\frac{1+r_{90}}{r_{90}}} \end{aligned} \tag{16}$$

The coefficient q should be calculated by a numerical procedure. Considering the principal directions of the stress tensor at the pole were coincident with the anisotropic axes of the

specimen during bulging processes in this work, stress components at the pole follow that $\sigma_{xx}=\sigma_{RD}$, $\sigma_{yy}=\sigma_{TD}$ and $\sigma_{xy}=0$. As a result, the coefficient q can be ignored. Barlat 1989 yield function coefficients for ST16 are given in Table 5.

Table 5. Barlat 1989 yield function coefficients for ST16.

a	c	h	M
0.612	1.388	0.951	6

The equivalent strain $\bar{\varepsilon}$ is defined using the plastic work rate equivalence [43,45]:

$$dW^p = \sigma_{RD} \cdot d\left(\varepsilon_{RD} - \varepsilon_{RD}^b\right) + \sigma_{TD} \cdot d\left(\varepsilon_{TD} - \varepsilon_{TD}^b\right) = \bar{\sigma} d\bar{\varepsilon} \tag{17}$$

Where dW^p is the plastic work increment and $d\bar{\varepsilon}$ is the equivalent strain increment.

Fig. 14 shows the equivalent stress-strain curves from uniaxial tension in RD, bulging with the circular die and bulging with different stepped-dies. It can be clearly found that curves $S_{1-0.4}^{0.1,R}$, $S_{1-0.4}^{0.1,T}$ and $S_{1-0.6}^{0.1,T}$ overshoot the curve E_1 after the bulging process transitions into step II and the loading path changes. The curve $S_{1-0.4}^{0.1,T}$ has the largest overshoot, while the curve $S_{1-0.6}^{0.1,R}$ is almost identical to the curve E_1. The curve from bulging with TD in the major axis is higher than that with RD in the major axis when bulging with the same die.

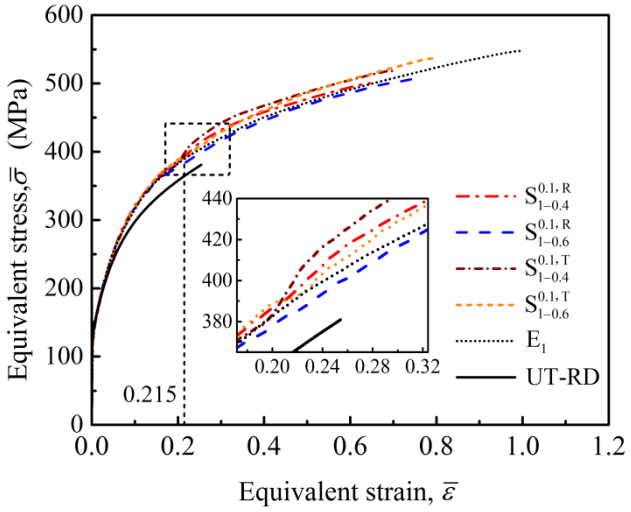

Fig. 14. Equivalent stress-strain curves.

According to the research performed by Barlat et al. [46], the latent hardening effect is

clearly identified in the EDDQ steel. The effect can lead to flow stress overshoot during two-step tension tests. As both ST16 and EDDQ belong to interstitial-free steel, ST16 also exhibits the latent hardening property. Due to the latent hardening effect, the equivalent stress of ST16 during step II of bulging with stepped-dies overshoots that of bulging with the circular die.

4.6 Future works

The new method, bulging with stepped-dies, was developed based on the traditional bulging test method. The key development in this work is that the section shape of a stepped-die cavity varies as the depth increases, which is different from the monotonous elliptical or circular die section in the traditional method. As a result, continuous nonlinear loading paths can be realized. Therefore, the new method is suitable for materials that can be tested using the traditional bulging test method, such as steel, Aluminum alloy, Magnesium alloy and Titanium alloy [15,16,21].

As a new test method, there are still significant further work needed to develop the process. In most cases it is helpful to accurately predict the stress path during bulging with a stepped-die without the use of finite element simulations and bulging experiments. Therefore, the relationship between the stress path and the cross section of the die cavity is an important topic to be clarified. Furthermore, the design method for a stepped-die should be investigated to induce favorable nonlinear stress paths. Moreover, more complex loading paths can be obtained through combining the new test method with pre-strains. Constitutive and forming limit models should be developed based on those experimental data under nonlinear loading paths, which will aid in modelling the material behavior in manufacturing processes.

5. Conclusions

In this paper, a novel test method named bulging with stepped-dies for continuous

nonlinear biaxial tensile deformation of sheet metals has been proposed. The feasibility of the method has been validated through bulging with three different stepped-dies. The following conclusions can be obtained from the study:

(1) Nonlinear loading paths can be effectively realized through bulging with stepped-dies. The curves of curvature radius and pole thickness versus bulging height change abruptly when the bulging process transits from an elliptical step into another elliptical step. The greater the difference between the two elliptical sections, the more obvious the nonlinearity of the stress and strain paths.

(2) The nonlinear loading path is determined by the change of cross section of the die cavity for a given sheet metal and its position relative to the die. Both the abrupt and smooth nonlinearity of loading path can be obtained by using an appropriately designed stepped-die.

(3) In one bulging experiment with a stepped-die, the stress ratio at the pole changes from 0.5 up to 2.0 at most, which corresponding to two different plane strain states.

(4) By using the new test method both the stress and strain data of the whole process from initial yield to fracture can be obtained. These data are useful to determine constitutive and forming limit models suitable for complex loading conditions.

(5) Fracture stresses are much less path-dependent than fracture strains. However, the path dependence of fracture stresses will become apparent if the strain level in the previous deformation is significant.

Acknowledgements

This work was financially supported by the National Natural Science Foundation of China (No. 51575131, U1637209), National Key R&D Program of China (2017YFB0304400, 2017YFB0306304). The authors would like to take this opportunity to express their sincere appreciation to the funds.

References

[1] Meinders T, Burchitz IA, Bonte MHA, Lingbeek RA. Numerical product design: Springback prediction, compensation and optimization. Int J Mach Tools Manuf 2008;48:499–514. doi:10.1016/j.ijmachtools.2007.08.006.

[2] Bouvier S, Gardey B, Haddadi H, Teodosiu C. Characterization of the strain-induced plastic anisotropy of rolled sheets by using sequences of simple shear and uniaxial tensile tests. J Mater Process Technol 2006;174:115–26. doi:10.1016/j.jmatprotec.2005.04.086.

[3] Haddadi H, Bouvier S, Banu M, Maier C, Teodosiu C. Towards an accurate description of the anisotropic behaviour of sheet metals under large plastic deformations: Modelling, numerical analysis and identification. Int J Plast 2006;22:2226–71. doi:10.1016/j.ijplas.2006.03.010.

[4] Kleemola, H.J., Pelkkikangas, M. T. Effect of predeformation and strain path on the forming limits of steel. Sheet Met Ind 1977;63:559–91.

[5] Zhalehfar F, Hashemi R, Hosseinipour SJ. Experimental and theoretical investigation of strain path change effect on forming limit diagram of AA5083. Int J Adv Manuf Technol 2014;76:1343–52. doi:10.1007/s00170-014-6340-3.

[6] Yoshida K, Kuwabara T, Narihara K, Takahashi S. Experimental verification of the path-independence of forming limit stresses. Int J Form Process 2005;8:283–98.

[7] Korkolis YP, Kyriakides S. Path-dependent failure of inflated aluminum tubes. Int J Plast 2009;25:2059–80. doi:10.1016/j.ijplas.2008.12.016.

[8] Olsen TY. Machines for ductility testing. Proc Am Soc Test Mater 1920;20:398–403.

[9] ISO 16808:2014. Metallic materials – sheet and strip – determination of biaxial stress-strain curve by means of bulge test with optical measuring systems. Int Organ Stand 2014.

[10] Reis LC, Prates PA, Oliveira MC, Santos AD, Fernandes J V. Anisotropy and plastic flow in the circular bulge test. Int J Mech Sci 2017;128–129:70–93. doi:10.1016/j.ijmecsci.2017.04.007.

[11] Chen K, Scales M, Kyriakides S. Material hardening of a high ductility aluminum alloy from a bulge test. Int J Mech Sci 2018;138–139:476–88. doi:10.1016/j.ijmecsci.2018.02.002.

[12] Marandi FA, Jabbari AH, Sedighi M, Hashemi R. An experimental, analytical, and numerical investigation of hydraulic bulge test in two-layer Al-Cu sheets. J Manuf Sci Eng Trans ASME 2017;139. doi:10.1115/1.4034717.

[13] Janbakhsh M, Djavanroodi F, Riahi M. Utilization of bulge and uniaxial tensile tests for determination of flow stress curves of selected anisotropic alloys. Proc Inst Mech Eng Part L J Mater Des Appl 2013;227:38–51. doi:10.1177/1464420712451963.

[14] Yousif MI, Duncan JL, Johnson W. Plastic deformation and failure of thin elliptical diaphragms. Int J Mech Sci 1970;12:959–72. doi:10.1016/0020-7403(70)90036-6.

[15] Chan KC, Chow KK. Analysis of hot limit strains of a superplastic 5083 aluminum alloy under biaxial tension. Int J Mech Sci 2002;44:1467–78. doi:10.1016/S0020-7403(02)00037-1.

[16] Abu-Farha F, Verma R, Hector LG. High temperature composite forming limit diagrams of four magnesium AZ31B sheets obtained by pneumatic stretching. J Mater Process Technol 2012;212:1414–29. doi:10.1016/j.jmatprotec.2012.01.008.

[17] Rees DWA. Plastic flow in the elliptical bulge test. Int J Mech Sci 1995;37:373–89. doi:10.1016/0020-7403(94)00071-Q.

[18] Lazarescu L, Nicodim IP, Comsa DS, Banabic D. A Procedure for the Evaluation of Flow Stress of Sheet Metal by Hydraulic Bulge Test Using Elliptical Dies. Key Eng Mater 2012;504–506:107–12. doi:10.4028/www.scientific.net/kem.504-506.107.

[19] Lăzărescu L, Comşa DS, Nicodim I, Ciobanu I, Banabic D. Characterization of plastic behaviour of sheet metals by hydraulic bulge test. Trans Nonferrous Met Soc China 2012;22:275–9. doi:10.1016/S1003-6326(12)61719-1.

[20] Lenzen M, Merklein M. Improvement of Numerical Modelling Considering Plane Strain Material Characterization with an Elliptic Hydraulic Bulge Test. J Manuf Mater Process 2018;2:6. doi:10.3390/jmmp2010006.

[21] Williams BW, Boyle KP. Characterization of anisotropic yield surfaces for titanium sheet using hydrostatic bulging with elliptical dies. Int J Mech Sci 2016;114:315–29. doi:10.1016/j.ijmecsci.2016.05.022.

[22] Sugawara F, Yoshida K, Kuwabara T, Taomoto N, Yanagi N. Forming limit prediction of sheet metals subjected to combined loading using forming limit stress curve. AIP Conf. Proc., vol. 1315, 2010, p. 383–8. doi:10.1063/1.3552473.

[23] Kuwabara T, Ikeda S, Kuroda K. Measurement and analysis of differential work hardening in cold-rolled steel sheet under biaxial tension. J Mater Process Technol 1998;80–81:517–23. doi:10.1016/S0924-0136(98)00155-1.

[24] Kuwabara T. Effect of Anisotropic Yield Functions on The Accuracy of Springback Simulation. AIP Conf. Proc. 2004, vol. 712, 2004, p. 887–92. doi:10.1063/1.1766639.

[25] KUWABARA T, NAKAJIMA T. Material Modeling of 980 MPa Dual Phase Steel Sheet Based on Biaxial Tensile Test and In-plane Stress Reversal Test. J Solid Mech Mater Eng 2011;5:709–20. doi:10.1299/jmmp.5.709.

[26] Kuroda M, Tvergaard V. Use of abrupt strain path change for determining subsequent yield surface: illustrations of basic idea. Acta Mater 1999;47:3879–90. doi:10.1016/S1359-6454(99)00213-X.

[27] Yu Y, Wan M, Wu XD, Zhou X Bin. Design of a cruciform biaxial tensile specimen for limit strain analysis by FEM. J Mater Process Technol 2002;123:67–70. doi:10.1016/S0924-0136(02)00062-6.

[28] Leotoing L, Guines D, Zidane I, Ragneau E. Cruciform shape benefits for experimental and numerical evaluation of sheet metal formability. J Mater Process Technol 2013;213:856–63. doi:10.1016/j.jmatprotec.2012.12.013.

[29] Liu W, Guines D, Leotoing L, Ragneau E. Identification of sheet metal hardening for large strains with an in-plane biaxial tensile test and a dedicated cross specimen. Int J Mech Sci 2015;101–102:387–98. doi:10.1016/j.ijmecsci.2015.08.022.

[30] Leotoing L, Guines D. Investigations of the effect of strain path changes on forming limit curves using an in-plane biaxial tensile test. Int J Mech Sci 2015;99:21–8. doi:10.1016/j.ijmecsci.2015.05.007.

[31] Sumita T, Kuwabara T, Hayashida Y. Measurement of work hardening behavior of pure titanium sheet using a servo-controlled tube bulge testing apparatus. AIP Conf Proc 2011;1353:1423–8. doi:10.1063/1.3589716.

[32] Kuwabara T, Sugawara F. Multiaxial tube expansion test method for measurement of sheet metal deformation behavior under biaxial tension for a large strain range. Int J Plast 2013;45:103–18. doi:10.1016/j.ijplas.2012.12.003.

[33] Kuwabara T, Ishiki M, Kuroda M, Takahashi S. Yield locus and work hardening behavior of a thin-walled steel tube subjected to combined tension-internal pressure. J Phys IV 2003;105:347–54. doi:10.1051/jp4:20030206.

[34] Kuwabara T, Yoshida K, Narihara K, Takahashi S. Anisotropic plastic deformation of extruded aluminum alloy tube under axial forces and internal pressure. Int J Plast 2005;21:101–17. doi:10.1016/j.ijplas.2004.04.006.

[35] Yoshida K, Kuwabara T. Effect of strain hardening behavior on forming limit stresses of steel tube

subjected to nonproportional loading paths. Int J Plast 2007;23:1260–84. doi:10.1016/j.ijplas.2006.11.008.

[36] Koç M, Billur E, Cora ÖN. An experimental study on the comparative assessment of hydraulic bulge test analysis methods. Mater Des 2011;32:272–81. doi:10.1016/j.matdes.2010.05.057.

[37] Reis LC, Oliveira MC, Santos AD, Fernandes J V. On the determination of the work hardening curve using the bulge test. Int J Mech Sci 2016;105:158–81. doi:10.1016/j.ijmecsci.2015.11.009.

[38] Wang Y, Yang L, Bai B, Lang L. Evaluation of limit deformation behavior in hydro-bulging of the double-layer sheet metal using diffuse and localized instability theories. Int J Mech Sci 2019;150:145–53. doi:10.1016/j.ijmecsci.2018.10.027.

[39] Min J, Stoughton TB, Carsley JE, Carlson BE, Lin J, Gao X. Accurate characterization of biaxial stress-strain response of sheet metal from bulge testing. Int J Plast 2017;94:192–213. doi:10.1016/j.ijplas.2016.02.005.

[40] Kaya S, Altan T, Groche P, Klöpsch C. Determination of the flow stress of magnesium AZ31-O sheet at elevated temperatures using the hydraulic bulge test. Int J Mach Tools Manuf 2008;48:550–7. doi:10.1016/j.ijmachtools.2007.06.011.

[41] Lenzen M, Merklein M. Improvement of the drawing ratio of the anisotropic material behaviour under near plane strain conditions for DP600 characterized in elliptic hydraulic bulge test. J Phys Conf Ser 2018;1063. doi:10.1088/1742-6596/1063/1/012161.

[42] Hora P, Tong L, Reissner J. A prediction method of ductile sheet metal failure in FE simulation. Proceeding NUMISHEET Conf., 1996, p. 252–256.

[43] Hora P, Tong L, Berisha B. Modified maximum force criterion, a model for the theoretical prediction of forming limit curves. Int J Mater Form 2013;6:267–79. doi:10.1007/s12289-011-1084-1.

[44] Barlat F, Lian J. Plastic behavior and stretchability of sheet metals. Part I: A yield function for orthotropic sheets under plane stress conditions. Int J Plast 1989;5:51–66.

[45] Hill R. Theoretical plasticity of textured aggregates. Math Proc Cambridge Philos Soc 1979;85:179–91. doi:10.1017/S0305004100055596.

[46] Barlat F, Ha J, Grácio JJ, Lee MG, Rauch EF, Vincze G. Extension of homogeneous anisotropic hardening model to cross-loading with latent effects. Int J Plast 2013;46:130–42. doi:10.1016/j.ijplas.2012.07.002.

Declaration of interests

 The authors declare that they have no known competing financial interests or personal relationships that could have appeared to influence the work reported in this paper.

☐The authors declare the following financial interests/personal relationships which may be considered as potential competing interests: